

Rydberg crystallization detection by statistical means

D. Breyel,¹ T. L. Schmidt,^{2,3} and A. Komnik¹

¹*Institut für Theoretische Physik, Universität Heidelberg,
Philosophenweg 19, D-69120 Heidelberg, Germany*

²*Department of Physics, Yale University, 217 Prospect Street, New Haven, CT 06520, USA*

³*Departement Physik, Universität Basel, Klingelbergstrasse 82, 4056 Basel, Switzerland*

(Dated: November 13, 2018)

We investigate an ensemble of atoms which can be excited into a Rydberg state. Using a disordered quantum Ising model, we perform a numerical simulation of the experimental procedure and calculate the probability distribution function $P(M)$ to create a certain number of Rydberg atoms M , as well as their pair correlation function. Using the latter, we identify the critical interaction strength above which the system undergoes a phase transition to a Rydberg crystal. We then show that this phase transition can be detected using $P(M)$ alone.

PACS numbers: 32.80.Rm, 75.10.Pq, 64.70.Tg, 34.20Cf

I. INTRODUCTION

Recent experimental progress in producing and controlling highly excited atomic and molecular aggregates have triggered a number of experimental and theoretical works on interacting Rydberg systems.^{1–16} One of the most prominent phenomena observable in such systems is the dipole blockade,^{17,18} which is a consequence of effective interactions between atoms in Rydberg states with principal quantum numbers $n \sim 30 - 80$.¹⁹ The physical reason for the blockade can be summarized as follows: the large dipole moment of a Rydberg atom induces sizeable energy level shifts in the atoms in its vicinity. As a result, atoms within a certain blockade radius R_B cannot be excited, even though they are subjected to the same electromagnetic field as the proper Rydberg atoms.

Typical experiments are conducted on atom ensembles at ultralow temperatures and probe these systems on timescales during which almost no particle movement is possible. Therefore, the cloud of atoms can be considered as ‘frozen’ in a more or less disordered constellation.²⁰ After the required fine-tuned electromagnetic fields are switched on, a number of atoms undergo a transition into the highly excited Rydberg states. If R_B is larger than the average interatomic distance, only a fraction of the atoms can be excited, while the rest remains in the ground state due to the blockade effect.

The spatial arrangement of the Rydberg atoms within the cloud has very interesting features. In Ref. [21], the concept of a Rydberg crystal was put forward. The blockade region formed around an excited atom can be modeled as an effective repulsive interaction between the Rydberg atoms. It might be responsible for an emergent long-range order of the Wigner crystal type²². However, its detection is extremely difficult. The primary method for detecting long-range order is spectroscopy, which is difficult to reliably realize in experiments.²³ Other experiments benefit from the low ionization energy of the Rydberg atoms by (pulsed) electric field ionization (cf. e.g. [7,11,13,14,17,19,20,24–38]).

In this paper we propose a statistical method of detecting and analyzing the physical properties of the Rydberg crystallization phenomenon and discuss its predictive power. The idea roots in the experimental procedure itself. A typical measurement cycle starts with the generation of an ultracold atomic cloud and the subsequent excitation of a fraction of the atoms to a Rydberg state. Afterwards, measurements are performed, during which the Rydberg atoms are eventually de-excited. Then, the system is ready for another preparation.^{30,32,38–40} An important point is that the experiments are performed with the same number of atoms and using the same electromagnetic fields in every cycle. However, since the arrangement of atoms varies between cycles, it is necessary to calculate statistical averages of the observables of interest. The simplest observable is the number of Rydberg atoms M in the cloud. The fact that for a given M , a regular arrangement of the Rydberg atoms on a lattice minimizes their interaction energy, should be visible in the probability distribution $P(M)$. As we shall show below there are indeed differences between the histograms for crystallized and random phases. However, the pair correlation function turns out to possess even higher predictive power.^{36,41}

This article is organized as follows. In Sec. II we shall introduce the model and connect its parameters to possible experimental setups. We shall define the relevant observables and explain the details of our numerical implementation. The results of the calculation together with a thorough analysis of the arising features is contained in Sec. III. Section IV is devoted to the summary of results.

II. THE MODEL AND SIMULATION METHOD

We assume that in every measurement cycle the system consists of N atoms located at randomly chosen positions $\mathbf{r}_i, i = 1, \dots, N$, uniformly distributed over the entire system volume.⁵¹ We focus on the case of a frozen Rydberg gas, where the kinetic energy is negligible. Each of the atoms can either be excited to a Rydberg state or stay in

its ground state. Since the electrostatic properties do not depend on the details of the Rydberg states, each atom can be modeled as a two-level system, and we describe the ensemble as a set of N randomly arranged, interacting spin-1/2 systems. Hence, the Hamiltonian reads⁴²

$$H = -\frac{\Delta}{2} \sum_{i=1}^N \sigma_z^{(i)} + \frac{\Omega}{2} \sum_{i=1}^N \sigma_x^{(i)} + \frac{C}{4} \sum_{i=2}^N \sum_{j=1}^{i-1} \frac{(1 + \sigma_z^{(i)})(1 + \sigma_z^{(j)})}{|\mathbf{r}_i - \mathbf{r}_j|^6}, \quad (1)$$

where $\sigma_{x,z}^{(i)}$ denote the Pauli matrices. This can be interpreted as a generalized spin-1/2 quantum Ising model. Ω is the frequency of the exciting laser and, in the spin language, represents a magnetic field perpendicular to the quantization axis, which we chose to be the z -axis. The detuning, i.e., the difference between the laser frequency to the resonance frequency of the Rydberg state, is denoted by Δ . It corresponds to a magnetic field applied in z -direction. The third parameter, C , indicates the strength of an effective interaction between excited atoms and causes the dipole blockade explained above.⁴³ We note that we are only interested in the case $\Delta > 0$, because otherwise it is energetically not favorable to excite atoms. This allows us to use Δ as a basic energy scale.

An adequate modeling of the system also requires geometrical constraints describing the trap potentials. In the following we shall consider different scenarios: (i) a 1D system with open boundaries,⁵² (ii) a 3D system with open boundaries, (iii) a 1D system with periodic boundary conditions. Options (i) and (ii) are very natural models for realistic experiments, but make it difficult to extrapolate the presented numerical results towards realistic system sizes. Option (iii), on the other hand, is perfectly suitable for the calculation of correlation functions and is easily scalable to large system lengths. The crucial feature of our 1D model is a rather large ‘‘coordination number’’, i.e., the number of atoms which interact significantly with any given Rydberg atom. This feature is shared by any generic 3D realization of the system up to some irrelevant spatial distribution parameter. That is why we believe that the physics in 3D is expected to be very similar to our 1D model.

Just as in the actual experiments we calculate averages over the large number of different, randomly sampled atom arrangements. In every cycle the effective model is a long-range quantum Ising model with a set of coupling constants generated by the atom positions \mathbf{r}_i . For every such constellation, we determine the ground state and evaluate the number of Rydberg atoms M (which is equivalent to the magnetization in the Ising model), the density profile and correlation functions. The most difficult task is finding the ground state. We use one method, numerical diagonalization of the Hamiltonian matrix, in three different variations. For small atom numbers ($N \approx 12$) the Hamiltonian can be diagonalized

exactly. For larger numbers of atoms ($N \approx 30$), we truncate the Hilbert space in different ways in order to speed up the numerical diagonalization. On the one hand, this truncation can be done by only keeping states in which the number of Rydberg atoms M remains below a certain threshold M^* . A different approach is to only use the basis states with the lowest energy expectation values to create an effective Hamiltonian, which is then diagonalized. We checked the reliability of both procedures by changing the respective cutoff parameter.

To calculate the number of Rydberg atoms and the correlation function we proceed as follows. For a given random distribution of atoms, the Hamiltonian matrix is expressed in a basis consisting of states in which an integer number of atoms is in the Rydberg state while the rest is in the ground state. The corresponding Hilbert space is then truncated as explained above, and the smallest eigenvalue and the corresponding eigenvector (the ground state $|GS\rangle$) are obtained numerically. The number of Rydberg atoms in the ground state is now found from

$$M = \sum_{i=0}^{\tilde{N}} M(i) |v_i|^2, \quad (2)$$

where \tilde{N} is the dimension of the truncated Hilbert space, $M(i) = \sum_{j=1}^N \langle i | (1 + \sigma_z^{(j)}) | i \rangle$ the number of Rydberg atoms in the basis state $|i\rangle$ and $v_i = \langle i | GS \rangle$ is the overlap between $|i\rangle$ and the ground state. One easy way of numbering the basis states is to assign a ‘‘1’’ to a Rydberg atom and a ‘‘0’’ to a ground state atom. In this way, every basis state can be uniquely mapped to the binary representation of a number $i \in \mathbb{N}_0$.

Furthermore, we calculate the pair correlation function

$$g(\mathbf{r}) = \langle \rho_{\text{Rydberg}}(\mathbf{r}) \rho_{\text{Rydberg}}(0) \rangle, \quad (3)$$

where $\rho_{\text{Rydberg}}(\mathbf{r}) d\mathbf{r}$ denotes the number of Rydberg atoms in a volume element $d\mathbf{r}$ around the point \mathbf{r} . The first step is to divide the interval of possible distances between two atoms ($[0; L/2]$ for periodic boundary conditions) into k subintervals of equal length. Calculating the ground state $|GS\rangle$ for a given distribution of atoms yields the coefficients v_i . Now, we consider a single pair of atoms and measure their distance in the current distribution of atoms. This distance lies within one of the aforementioned subintervals. To the value which is already stored for this subinterval we now add the sum of all $|v_i|^2$ that correspond to a basis state in which both of the atoms of the considered pair are in the Rydberg state. After repeating this procedure for every possible pair of atoms we start over by generating a new random distribution. The cumulative sum of all samples treated this way then gives the total correlation function for a given set of parameters.

III. RESULTS AND DISCUSSION

Let us first discuss the simplest case of a noninteracting system, $C = 0$. In this case, the problem is exactly solvable and the number of Rydberg atoms is given by

$$M_0 = \frac{N}{2} \left(1 + \frac{1}{\sqrt{1 + \Omega^2/\Delta^2}} \right). \quad (4)$$

In the noninteracting limit, this value is independent of the positions \mathbf{r}_i of the atoms. Therefore, the histogram $P(M)$ becomes trivial, $P(M) = \delta(M - M_0)$. The density distribution $\rho_0 = \langle \rho_{\text{Rydberg}}(\mathbf{r}) \rangle$, averaged over many realizations, is uniform, and the pair correlation function $g(\mathbf{r}) = \rho_0^2$ is constant.

The situation changes drastically for any nonzero C . Figure 1 shows the data for the density distribution $\langle \rho_{\text{Rydberg}}(\mathbf{r}) \rangle$ in 1D and 3D systems with open boundaries. While for weak interactions the Rydberg atoms tend to populate the boundaries, in the case of strong interactions a sizeable fraction of the atoms is redistributed towards the system's bulk, indicating that long-range order is established in the system. As we are dealing with a system with long-range interactions, the numerical complexity is determined by the number of Rydberg atoms and not by the precise geometry of the system. On the other hand, going to higher dimensions at fixed atom number N increases the surface/bulk ratio and thus makes the detection of long-range order more cumbersome. Therefore we shall concentrate on (quasi)-1D systems from now on. Nonetheless, we have conducted a number of simulations on 3D systems and found comparable results, see e.g., Fig. 1 for the density profile of a 3D system. We also would like to remark that an experimentally realizable cigar-shaped confining potential (with a typical radius smaller than R_B) can be very well be approximated by the (quasi)-1D geometry considered here.

Figure 2 shows a typical result for the histogram $P(M)$. For $\Omega = 0$, the number of Rydberg atoms commutes with the Hamiltonian, so the ground state for a given set of position $\{\mathbf{r}_i\}$ has an integer expectation value M of Rydberg atoms. The distribution $P(M)$, generated by considering all arrangements $\{\mathbf{r}_i\}$, thus becomes a series of discrete, weighted peaks at integer values M . For small $0 < \Omega \ll \Delta$, these peaks broaden up, but the distribution remains more or less discrete. Increasing Ω leads to further broadening until eventually a continuous distribution is approached, see inset of Fig. 2.

Surprisingly, in most cases the envelope of the histogram can fairly well be fitted by a Gaussian, as opposed to the Poissonian used, e.g., in Ref. [29]. Nonetheless, the distribution function's higher order cumulants are not exactly zero and depend on C , which indicates a slight deviation from the Gaussian distribution. The mean μ and the variance σ for a series of simulations are plotted in Fig. 3. Very interestingly, the $\mu(C)$ dependence is given by a power law with an exponent which

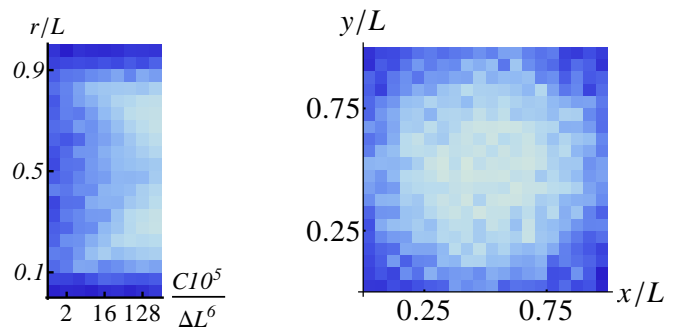


FIG. 1: Density distribution of Rydberg atoms, darker color indicates higher density. *Left panel*: 1D density as a function of interaction strength. The system boundaries are preferred. Strong interactions produce a single peak in the center. *Parameters*: $\Omega/\Delta = 0.1$ and $N = M^* = 6$ atoms (no cutoff, exact diagonalization). *Right panel*: 2D projection of a 3D system with $N = M^* = 6$, $\Omega/\Delta = 4$ and $C = 10$ in a cube with open boundaries. There is a low density at the center of the volume while it is high in the corners.

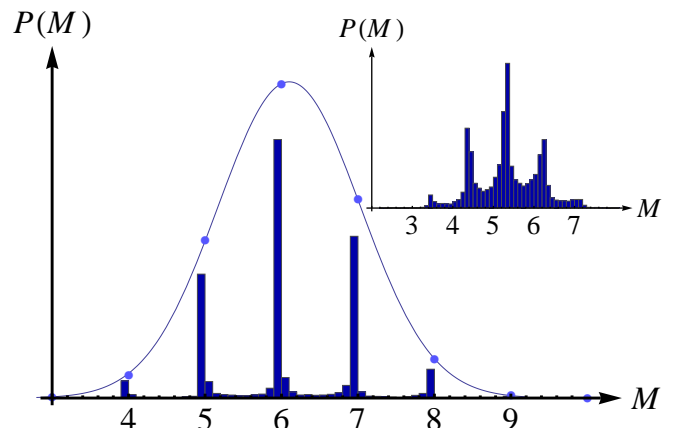


FIG. 2: *Main figure*: Histogram of the number of Rydberg atoms with Gaussian fit. The data points shown are the cumulative sum of all bins in the interval $[n - 0.5, n + 0.5]$. The features of the plot are explained in the text. *Parameters*: $\Omega/\Delta = 0.1$, $C/(\Delta L^6) = 4 \cdot 10^{-7}$ with $N = 10 = M^*$ atoms (which corresponds to no cut-off). *Inset*: Histogram for $\Omega/\Delta = 0.64$, $C/(\Delta L^6) = 5 \cdot 10^{-7}$ with $N = 10 = M^*$ atoms.

changes abruptly from ≈ -0.05 to ≈ -0.1 at around $C/(\Delta L^6) \approx 10^{-6}$, where L is the system length. We find this change to be a harbinger of a phase transition in the system. Both the mean and the width of the distribution function decrease as a function of C because a stronger repulsion increases the blockade radius R_B . This qualitative behavior is independent of the value of Ω .

If one plots the mean and the variance as functions of Ω the general behavior of the mean $\mu(\Omega)$ is qualitatively the same as for the noninteracting case [$\mu(\Omega) = \mu(\Omega, C = 0)$; cf. Eq. (4)] for $\Omega < \Omega^*$, where $\Omega^* = \max(C/L^6, \Delta)$ is the largest energy scale in the system. For $\Omega > \Omega^*$ the spin flip term dominates the Hamiltonian (1) and M tends to

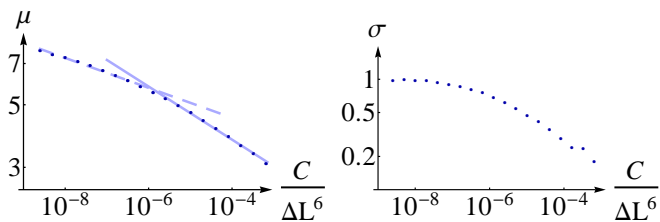


FIG. 3: Average number of Rydberg atoms μ (left) and variance σ (right) in dependence on C (double-log-plots). The straight lines in the average number of Rydberg atoms plot are guides to the eye only. The parameters for all three plots are $\Omega/\Delta = 0.2$ with $N = 10 = M^*$ atoms. The resulting Mandel parameter is displayed in Fig. 4.

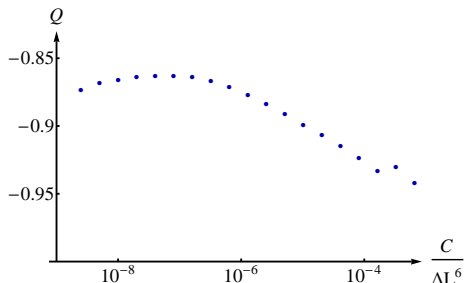


FIG. 4: Mandel Q parameter in dependence on the interaction strength C . The data points are calculated using the data from Fig. 3.

$N/2$. The only effect of C is the change in the overall amplitude of the curve.

To quantify the deviation of $P(M)$ from a Poissonian distribution we use the Mandel Q parameter which is defined as⁴⁴

$$Q = \frac{\langle M^2 \rangle - \langle M \rangle^2}{\langle M \rangle} - 1. \quad (5)$$

It is plotted in Fig. 4 for the same series of simulations. Being negative throughout, it indicates that the $P(M)$ distribution is sub-Poissonian.^{45,46} As realized in Ref. [29] this points towards an efficient Rydberg blockade.

Another interesting quantity is the pair correlation function $g(r)$, which is defined as the probability to find a Rydberg atom at a distance r from another Rydberg atom. In order to exclude boundary effects, we now switch to periodic boundary conditions. To be able to handle computations with larger numbers of atoms we change the truncation procedure to one in which we consider only a fixed number of basis states. This enables us to approach $N \approx 30$. This set of states is chosen to be the one with the smallest diagonal elements in the Hamiltonian matrix. We thoroughly investigated the effect of the truncation by considering the same system with different numbers of contributing states. We find that the result is almost independent of the number of states as long as it exceeds a certain threshold. All plots displayed in this paper meet this requirement.

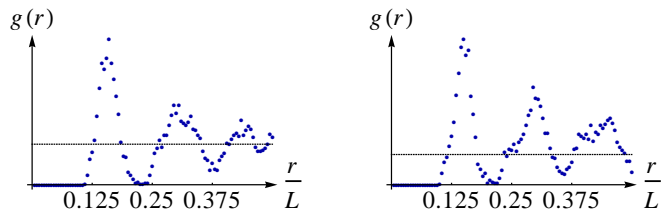


FIG. 5: *Left*: Correlation function with adjustment of the system length in such a way that main and secondary peaks coincide, $C/(\Delta L^6) = 7.5 \cdot 10^{-6}$. *Right*: Correlation function as a function of distance. The aliasing can be seen in the shoulders of the second and third maximum, $C/(\Delta L^6) = 4 \cdot 10^{-6}$. For both correlation functions $N = 30$ and $\Omega/\Delta = 25$.

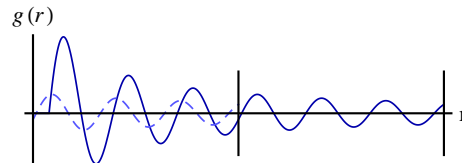


FIG. 6: Schematic illustration of the effect shown in Fig. 5. The dashed line is part of the correlation function in the right interval shifted by the length of the interval. The sum of dashed and solid curve in the left interval is a curve with main peaks that have secondary peaks on their shoulders. The secondary peak on the shoulder of the first peak is suppressed because of the blockade phenomenon.

A typical correlation function is shown in Fig. 5 and is qualitatively comparable to the ones shown in Ref. [16]. On the right panel one can see additional smaller peaks, which originate from the periodic boundary conditions, on the left side of two principal peaks. This feature, which is known as “aliasing”, arises in the following way: in the plots shown in Fig. 5 (and in any other plot of a correlation function in this work) our domain of definition is the interval $[0, L/2]$ since $L/2$ is the maximum distance between two atoms in a 1D system with periodic boundary conditions. Now we could extrapolate this correlation function for larger distances. Since we are not able to resolve those the correlation function is mapped onto the given interval periodically. So the additional peaks appearing here are basically the 5th and 6th order peaks of the correlation function. Fig. 6 illustrates this behaviour, which is also known from the numerical realization of Fourier transforms with finite frequency cutoff.⁴⁷ This effect can be hidden when one uses such parameter values at which L and R_B are commensurate, see the left panel of Fig. 5. Using this control prescription we have calculated $g(r)$ for a very large number of samples for a number of different interaction strengths, see Fig. 9.

As expected, one can immediately identify the blockade radius R_B as the position of the first maximum. It is the distance between two atoms up to which it is disadvantageous to excite both of them to the Rydberg state.

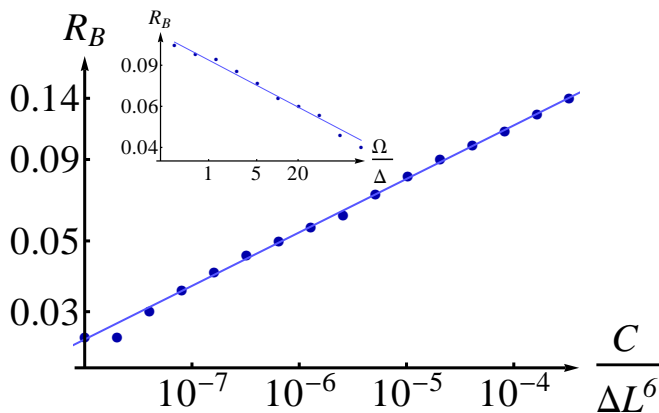


FIG. 7: *Main graph*: R_B as a function of C (double-log-plot). The data points clearly show a power law. The parameters are: $\Omega/\Delta = 0.1$ with $N = 8 = M^*$ atoms. The fit is discussed in the text. *Inset*: R_B as a function of Ω (double-log-plot). The parameters are: $C/(\Delta L^6) = 10^{-5}$ with $N = 7 = M^*$ atoms.

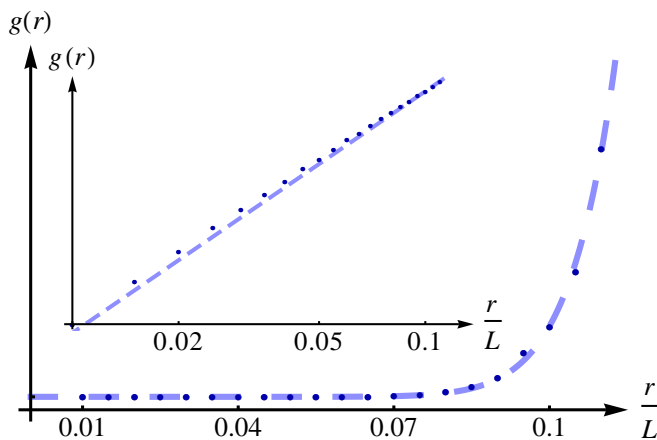


FIG. 8: *Main graph*: Correlation function as a function of distance. The dashed line represents a fit explained in the text. *Inset*: The same plot as in the main plot shown on a logarithmic scale. The parameters of the plot are: $\Omega/\Delta = 1$, $C/(\Delta L^6) = 2 \cdot 10^{-5}$ with $N = 6 = M^*$ atoms.

Obviously, it is nonzero for all interaction strengths C . The actual $R_B(C)$ dependence is very interesting and is plotted in Fig. 7. Very naturally, R_B grows with interaction strength as

$$R_B \approx (C/\Delta L^6)^\gamma, \quad (6)$$

where $\gamma \approx 1/6 \pm 1\%$. This was also discussed in Refs. [13,36,48,49]. Furthermore, we find the asymptotic behavior of the correlation function for $r \ll R_B$ to be highly universal (see Fig. 8). It is given by

$$g(r) \propto r^{12}, \quad r \ll R_B \quad (7)$$

which is in contrast to the step-like behavior found in Ref. [16]. Beyond the point $r = R_B$ the qualitative shape of $g(r)$ depends strongly on C . While for weak

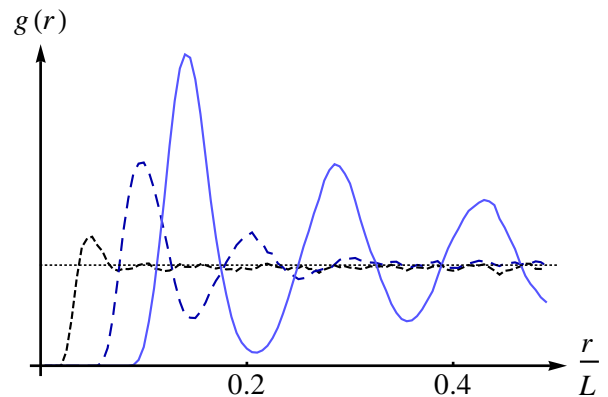


FIG. 9: Correlation function of 1D samples measured in arbitrary units. The curves correspond to $C/\Delta L^6 = 4 \cdot 10^{-9}$ (dotted), $C/\Delta L^6 = 4 \cdot 10^{-7}$ (dashed) and $C/\Delta L^6 = 4 \cdot 10^{-6}$ (solid) where all other parameters remained the same: $\Omega/\Delta = 1$ and $N = 25$ with 300 basis states. The curves indicate that there is a critical value for $C/\Delta L^6$ between the two larger values given above.

interactions, $C/(\Delta L^6) < 4 \cdot 10^{-9}$, no additional peaks can be seen, long-range order emerges for strong interactions $C/(\Delta L^6) > 10^{-6}$, and manifests itself as a series of equidistant peaks. In the former case, the Rydberg atoms remain in a gas phase, whereas the latter situation might be described as the Rydberg crystal proposed in Refs. [21,50]. In an ideal crystal, the additional peaks would be sharp. In our calculations this cannot be achieved due to finite-size effects. From our simulations we estimate the dimensionless critical parameter for the transition as $C_{\text{crit}}/(\Delta L^6) \approx 5 \cdot 10^{-7}$.

In fact, one can recognize this critical value for the phase transition already in the simple statistical parameter of the $P(M)$ histograms. Indeed, not only the mean value μ , but also the variance and Mandel parameter Q remarkably change their behavior near the critical value C_{crit} . For instance, Q is roughly constant for $C < C_{\text{crit}}$ but starts to decrease just below C_{crit} , see Fig. 4. The same happens to the variance. The behavior of μ is less prominent but still clearly detectable. Similar behavior can be seen in higher cumulants of $P(M)$. However, the larger statistical errors might make them less useful in practical applications.

IV. CONCLUSIONS

Using exact numerical diagonalization and approximate descendants of this method we have investigated the Rydberg crystallization phenomenon in ultracold gases. We have estimated the critical interaction strength by two different techniques. Both pair correlation function and simpler statistical data show signatures of this phase transition. The big advantage of using mean and variance of the histogram for the number of excited atoms measured in a long series of identical experiments is its

good experimental accessibility. In this way we have developed a purely statistical method of detecting Rydberg crystallization. We hope that this procedure can soon be implemented in state-of-the-art experiments in order to unambiguously identify the Rydberg crystallization phenomenon without complicated spectroscopic techniques.

Furthermore, the presented details of the pair correlation function might be useful for the continuous experimental efforts in spatial imaging of Rydberg aggregates in the spirit of Refs. [36,41]. This technique is not only able to yield very precise value of the blockade radius, but has also proven to be a reliable source for the estimation

of the critical parameters for Rydberg crystallization.

Acknowledgments

The authors would like to thank G. Günther, M. Weidemüller and S. Whitlock for many interesting discussions. AK is supported by the DFG Grant No. KO-2235/3-1, CQD and ‘Enable fund’ of the University of Heidelberg.

-
- ¹ S. Wüster, J. Stanojevic, C. Ates, T. Pohl, P. Deuar, J. F. Corney, and J. M. Rost, *Phys. Rev. A* **81**, 023406 (2010).
 - ² C. Ates, S. Sevinli, and T. Pohl, *Phys. Rev. A* **83**, 041802 (2011).
 - ³ C. Ates, T. Pohl, T. Pattard, and J. M. Rost, *Phys. Rev. A* **76**, 013413 (2007).
 - ⁴ F. Robicheaux, J. V. Hernández, T. Topçu, and L. D. Noordam, *Phys. Rev. A* **70**, 042703 (2004).
 - ⁵ S. Ji, C. Ates, and I. Lesanovsky, *Phys. Rev. Lett.* **107**, 060406 (2011).
 - ⁶ E. Urban, T. A. Johnson, T. Henage, L. Isenhower, D. D. Yavuz, T. G. Walker, and M. Saffman, *Nature Physics* **5**, 110 (2009).
 - ⁷ R. Löw, H. Weimer, U. Krohn, R. Heidemann, V. Bendkowsky, B. Butscher, H. P. Büchler, and T. Pfau, *Phys. Rev. A* **80**, 033422 (2009).
 - ⁸ T. A. Johnson, E. Urban, T. Henage, L. Isenhower, D. D. Yavuz, T. G. Walker, and M. Saffman, *Phys. Rev. Lett.* **100**, 113003 (2008).
 - ⁹ T. Amthor, C. Giese, C. S. Hofmann, and M. Weidemüller, *Phys. Rev. Lett.* **104**, 013001 (2010).
 - ¹⁰ N. Samboy, J. Stanojevic, and R. Côté, *Phys. Rev. A* **83**, 050501 (2011).
 - ¹¹ C. S. E. van Ditzhuijzen, A. F. Koenderink, J. V. Hernández, F. Robicheaux, L. D. Noordam, and H. B. v. L. van den Heuvel, *Phys. Rev. Lett.* **100**, 243201 (2008).
 - ¹² A. Wetzels, A. Gürtler, L. D. Noordam, and F. Robicheaux, *Phys. Rev. A* **73**, 062507 (2006).
 - ¹³ R. Heidemann, U. Raitzsch, V. Bendkowsky, B. Butscher, R. Löw, L. Santos, and T. Pfau, *Phys. Rev. Lett.* **99**, 163601 (2007).
 - ¹⁴ U. Raitzsch, V. Bendkowsky, R. Heidemann, B. Butscher, R. Löw, and T. Pfau, *Phys. Rev. Lett.* **100**, 013002 (2008).
 - ¹⁵ K. P. Heeg, M. Gärtner, and J. Evers, *ArXiv e-prints* (2012), 1202.2779.
 - ¹⁶ C. Ates and I. Lesanovsky, *ArXiv e-prints* (2012), 1202.2012.
 - ¹⁷ D. Tong, S. M. Farooqi, J. Stanojevic, S. Krishnan, Y. P. Zhang, R. Côté, E. E. Eyler, and P. L. Gould, *Phys. Rev. Lett.* **93**, 063001 (2004).
 - ¹⁸ M. D. Lukin, M. Fleischhauer, R. Cote, L. M. Duan, D. Jaksch, J. I. Cirac, and P. Zoller, *Phys. Rev. Lett.* **87**, 037901 (2001).
 - ¹⁹ K. Singer, M. Reetz-Lamour, T. Amthor, L. G. Marcassa, and M. Weidemüller, *Phys. Rev. Lett.* **93**, 163001 (2004).
 - ²⁰ I. Mourachko, D. Comparat, F. de Tomasi, A. Fioretti, P. Nosbaum, V. M. Akulin, and P. Pillet, *Phys. Rev. Lett.* **80**, 253 (1998).
 - ²¹ J. Schachenmayer, I. Lesanovsky, A. Micheli, and A. J. Daley, *New Journal of Physics* **12**, 103044 (2010).
 - ²² E. Wigner, *Phys. Rev.* **46**, 1002 (1934).
 - ²³ L. Jin, M. Macovei, and J. Evers, *ArXiv e-prints* (2012), 1202.0699.
 - ²⁴ C. Fabre, S. Haroche, and P. Goy, *Phys. Rev. A* **18**, 229 (1978).
 - ²⁵ T. Amthor, M. Reetz-Lamour, S. Westermann, J. Denskat, and M. Weidemüller, *Phys. Rev. Lett.* **98**, 023004 (2007).
 - ²⁶ W. R. Anderson, J. R. Veale, and T. F. Gallagher, *Phys. Rev. Lett.* **80**, 249 (1998).
 - ²⁷ C. Boisseau, I. Simbotin, and R. Côté, *Phys. Rev. Lett.* **88**, 133004 (2002).
 - ²⁸ T. J. Carroll, K. Claringbould, A. Goodsell, M. J. Lim, and M. W. Noel, *Phys. Rev. Lett.* **93**, 153001 (2004).
 - ²⁹ T. Cubel Liebisch, A. Reinhard, P. R. Berman, and G. Raithel, *Phys. Rev. Lett.* **95**, 253002 (2005).
 - ³⁰ A. Fioretti, D. Comparat, C. Drag, T. F. Gallagher, and P. Pillet, *Phys. Rev. Lett.* **82**, 1839 (1999).
 - ³¹ S. D. Hogan, P. Allmendinger, H. Saßmannshausen, H. Schmutz, and F. Merkt, *Phys. Rev. Lett.* **108**, 063008 (2012).
 - ³² M. Mudrich, N. Zahzam, T. Vogt, D. Comparat, and P. Pillet, *Phys. Rev. Lett.* **95**, 233002 (2005).
 - ³³ A. L. de Oliveira, M. W. Mancini, V. S. Bagnato, and L. G. Marcassa, *Phys. Rev. Lett.* **90**, 143002 (2003).
 - ³⁴ J. M. Raimond, G. Vitrant, and S. Haroche, *Journal of Physics B: Atomic and Molecular Physics* **14**, L655 (1981).
 - ³⁵ H. Schempp, G. Günter, C. S. Hofmann, C. Giese, S. D. Saliba, B. D. DePaola, T. Amthor, M. Weidemüller, S. Sevinli, and T. Pohl, *Phys. Rev. Lett.* **104**, 173602 (2010).
 - ³⁶ A. Schwarzkopf, R. E. Sapiro, and G. Raithel, *Phys. Rev. Lett.* **107**, 103001 (2011).
 - ³⁷ T. Vogt, M. Viteau, A. Chotia, J. Zhao, D. Comparat, and P. Pillet, *Phys. Rev. Lett.* **99**, 073002 (2007).
 - ³⁸ T. Vogt, M. Viteau, J. Zhao, A. Chotia, D. Comparat, and P. Pillet, *Phys. Rev. Lett.* **97**, 083003 (2006).
 - ³⁹ A. Chotia, M. Viteau, T. Vogt, D. Comparat, and P. Pillet, *New Journal of Physics* **10**, 045031 (2008).
 - ⁴⁰ M. Weidemüller, *Nature Physics* **5**, 91 (2009).
 - ⁴¹ G. Günter, M. Robert-de-Saint-Vincent, H. Schempp, C. S. Hofmann, S. Whitlock, and M. Weidemüller, *Physical Review Letters* **108**, 013002 (2012), 1106.5443.

- ⁴² F. Robicheaux and J. V. Hernández, *Phys. Rev. A* **72**, 063403 (2005).
- ⁴³ T. Amthor, M. Reetz-Lamour, and M. Weidemüller, *Cold Atoms and Molecules: Concepts, Experiments and Applications to Fundamental Physics* (Wiley-VCH, Berlin, 2009).
- ⁴⁴ L. Mandel, *Opt. Lett.* **4**, 205 (1979).
- ⁴⁵ C. Ates, T. Pohl, T. Pattard, and J. M. Rost, *Journal of Physics B: Atomic, Molecular and Optical Physics* **39**, L233 (2006).
- ⁴⁶ J. V. Hernández and F. Robicheaux, *Journal of Physics B: Atomic, Molecular and Optical Physics* **39**, 4883 (2006).
- ⁴⁷ W. H. Press, S. A. Teukolsky, W. T. Vetterling, and B. P. Flannery, *Numerical Recipes 3rd Edition: The Art of Scientific Computing* (Cambridge University Press, New York, NY, USA, 2007), 3rd ed., ISBN 0521880688, 9780521880688.
- ⁴⁸ S. Sevinçli, N. Henkel, C. Ates, and T. Pohl, *Physical Review Letters* **107**, 153001 (2011), 1106.2001.
- ⁴⁹ J. D. Pritchard, D. Maxwell, A. Gauguet, K. J. Weatherill, M. P. A. Jones, and C. S. Adams, *Phys. Rev. Lett.* **105**, 193603 (2010).
- ⁵⁰ T. Pohl, E. Demler, and M. D. Lukin, *Phys. Rev. Lett.* **104**, 043002 (2010).
- ⁵¹ This marks a difference to the recent publication [21], which used a lattice.
- ⁵² We allow for interactions to act ‘through’ the particles, that is why it is more appropriate to talk about quasi-1D systems rather than 1D ones.